Departement für Pferde, Abteilung für Ophthalmologie
der Vetsuisse-Fakultät Universität Zürich

Direktor: Prof. Dr. med. vet. Colin Schwarzwald, PhD, DACVIM, DECEIM
Leiter: Prof. Simon Pot, DVM, DACVO, DECVO

Arbeit unter wissenschaftlicher Betreuung von
Prof. Simon Pot, DVM, DACVO, DECVO

Interspecies Variation of Outer Retina and Choriocapillaris Imaged with Optical Coherence Tomography (OCT)

Inaugural-Dissertation

zur Erlangung der Doktorwürde der
Vetsuisse-Fakultät Universität Zürich

vorgelegt von

Petr Soukup

Tierarzt
von Frýdlant, Tschechische Republik

genehmigt auf Antrag von
Prof. Simon Pot, DVM, DACVO, DECVO

2019

Inhaltsverzeichnis

1 Summary

Purpose: To assess interspecies variation in outer retinal morphology and choriocapillaris identification in four research animal species with optical coherence tomography.

Methods: OCT images acquired from locations dorsal, central and ventral to the optic disc in healthy, anesthetized animals were evaluated by two independent readers. The number of B-scans on which choriocapillaris could be identified was determined and quantified and B-scans were correlated with histology. B-scans demonstrating the highest number of discernable outer retinal bands (ORB) were defined as ideal presentation and quantified. Interrater agreement was evaluated.

Results: Altogether 574 B-scans were evaluated. The choriocapillaris layer was identified in 100% of minipig, 70.8% of rabbit, 75.4% of pigmented rat, 77.7% of albino rat, 56.5% of pigmented mouse and 50.8% of albino mouse OCT scans. The percentage of optimal ORB presentation on B-scans was 11.7% in minipigs, 73.8% in rabbits and 80.0, 91.0, 28.5 and 62.5 % in pigmented rats and mice and albino rats and mice, respectively. The interrater evaluation for both endpoints showed agreement in all species.

Conclusion: The choriocapillaris is a valid marker for identification of the outer retinal margin. ORB presentation likely varies due to differences in retinal anatomy and pigmentation between animal species and strains. Proper and consistent outer retinal margin and ORB identification are essential for research reproducibility and translation.

Keywords: Outer retinal margin, outer retinal bands, choriocapillaris, optical coherence tomography, SD-OCT, rabbit, mouse, rat, minipig

2 Zusammenfassung

Zielsetzung: Untersuchung der Variabilität der äussere Retina Morphologie und Sichtbarkeit der Choriocapillaris (CC) mittels optischer Kohärenztomographie (OCT) bei vier unterschiedlichen Versuchstierarten.

Methoden: Dorsal, zentral und ventral der Sehnervenkopf lokalisierte OCT-Bilder von gesunden Tieren wurden von zwei unabhängigen Gradern ausgewertet. Die Anzahl Bilder, auf denen eine CC identifiziert wurde, ist quantifiziert. B-Scans mit der höchsten Anzahl erkennbaren äusseren Retinabände (ORB) wurden als ideale Präsentation definiert und quantifiziert. OCT Bilder wurden mit Histologie verglichen und die Interrater-Agreement bewertet.

Ergebnisse: Insgesamt 574 B-Scans wurden ausgewertet. Die CC war in 100% der Minipigs, 70.8% der Kaninchen, 75.4% der pigmentierten Ratten, 77.7% der Albinoratten, 56.5% der pigmentierten Mäusen und 50,8% der Albinomäusen sichtbar. Eine ideale ORB-Präsentation wurde in 11.7% der Minipigs, 73.8% der Kaninchen und 80.0, 91.0, 28.5 und 62.5% der pigmentierten Ratten und Mäusen bzw. Albinoratten und Mäusen bestimmt. Die Interrater-Agreement für die beide Endpunkte war erheblich bis perfekt.

Fazit: Die CC erscheint als zuverlässiger Marker der äusseren Netzhautbegrenzung (ORG). Die ORB-Darstellung variiert wahrscheinlich aufgrund der unterschiedliche Netzhautanatomie und Pigmentierung zwischen Tierarten. Eine korrekte Identifizierung der ORG und ORB sind für die Reproduzierbarkeit und Translation Forschungsergebnisse von grosser Bedeutung.

Schlagwörter: Äussere Netzhautbegrenzung, äussere Retinabänder, Choriocapillaris, optische Kohärenztomographie, SD-OCT, Kaninchen, Maus, Ratte, Minipig, Minischwein

3 Abdruck des gedruckten Artikels im Format der Fachzeitschrift IOVS

Interspecies Variation of Outer Retina and Choriocapillaris Imaged With Optical Coherence Tomography

Petr Soukup,[1,2] Peter Maloca,[3–5] Bernd Altmann,[1] Matthias Festag,[1] Elke-Astrid Atzpodien,[1] and Simon Pot[2]

[1]Roche Pharmaceutical Research and Early Development, Pharmaceutical Sciences, Roche Innovation Center, Basel, Switzerland
[2]Ophthalmology Section, Equine Department, Vetsuisse Faculty, University of Zurich, Zurich, Switzerland
[3]Institute of Molecular and Clinical Ophthalmology Basel (IOB), Basel, Switzerland
[4]OCTlab Research Laboratory, Department of Ophthalmology, University of Basel, Basel, Switzerland
[5]Moorfields Eye Hospital, London, United Kingdom

Correspondence: Petr Soukup, Ophthalmology Section, Vetsuisse Faculty, University of Zurich, Winterthurerstrasse 260, Zurich 8057, Switzerland; petr.soukup@uzh.ch.

PS and PM contributed equally to the work presented here and should therefore be regarded as equivalent first authors.

Submitted: November 28, 2018
Accepted: June 29, 2019

Citation: Soukup P, Maloca P, Altmann B, Festag M, Atzpodien E-A, Pot S. Interspecies variation of outer retina and choriocapillaris imaged with optical coherence tomography. *Invest Ophthalmol Vis Sci*. 2019;60:3332–3342. https://doi.org/10.1167/iovs.18-26257

Purpose. The purpose of this study is to assess with spectral-domain optical coherence tomography (OCT) the interspecies variation of outer retinal morphology and identification of choriocapillaris in four research animal species.

Methods. Spectralis HRA+OCT images acquired from locations dorsal, central, and ventral to the optic disc in healthy, anesthetized animals were evaluated by two independent readers. First, the number of OCT B-scans on which a choriocapillaris layer could clearly be identified was determined and quantified, and B-scans were correlated with histology. Second, B-scans demonstrating the highest number of discernable individual outer retinal bands (ORBs) were defined as ideal presentation and quantified. Interrater agreement was evaluated.

Results. Five-hundred seventy-four B-scans from 96 subjects were evaluated. The choriocapillaris layer was identified in 100.0% of minipig, 70.8% of rabbit, 75.4% of pigmented rat, 77.7% of albino rat, 56.5% of pigmented mouse, and 50.8% of albino mouse OCT scans. The percentage of ideal ORB presentation in B-scans was 11.7% in minipigs, 73.8% in rabbits, and 80.0%, 91.0%, 28.5%, and 62.5% in pigmented rats and mice and albino rats and mice, respectively. The interrater evaluation for both attributes showed substantial to perfect agreement in all species.

Conclusions. The choriocapillaris is an easy and valid marker for identification of the outer retinal margin. ORB presentation likely varies due to differences in retinal anatomy and pigmentation between animal species and strains and between anatomic locations. Proper and consistent outer retinal margin and ORB identification are essential for research result reproducibility and translation.

Keywords: outer retina, outer retinal bands, choriocapillaris, optical coherence tomography, SD-OCT, rabbit, mouse, rat, minipig

Optical coherence tomography (OCT) is a noninvasive in vivo imaging technique used extensively to visualize the posterior segment of the eye[1] and has become the standard of retinal imaging in preclinical ophthalmic research involving research animals.[2–4]

The outer retina is the area occupied by the photoreceptor inner and outer segments (OS) and RPE and is defined by the external limiting membrane (ELM) internally and by the RPE/Bruch's membrane complex (RPE/BM) externally. Four distinct hyperreflective outer retinal bands (ORBs) can be distinguished in humans using spectral domain OCT (SD-OCT).[5] These hyperreflective bands have been under vigorous investigation to determine their correct origin and correlation to histologic layers.[6–8] Although scientific unity has not been reached yet,[9–11] a consensus statement regarding the nomenclature of the hyperreflective bands that can be distinguished on OCT in the outer retina in humans was developed.[12] The nomenclature described in this consensus statement is listed in Table 1 and used throughout this paper.

Outer retinal band integrity and outer retinal thickness as they appear on OCT have been studied extensively due to their prognostic value, being predictive of visual outcome in many retinal diseases like AMD, diabetic retinopathy, retinal detachment, or retinal degeneration.[13–16]

Mice[17–20] and rats[21–24] are commonly used in preclinical ophthalmic research. Less frequently used species include nonhuman primates,[25–27] rabbits,[28–31] pigs,[32,33] minipigs,[34] guinea pigs,[35] dogs, cats,[36–38] tree shrews,[39] gerbils,[40] and ground squirrels.[41] Frogs[42–44] and zebrafish[45,46] are the more commonly used nonmammalian species. Despite the common use of various animal species in preclinical ophthalmic research involving OCT, no consensus exists regarding the nomenclature of the outer retinal bands (ORBs) distinguishable on OCT in different species. On the contrary, the identification/nomenclature of ORB and the definition of the retinal/choroidal junction on OCT in various species in the scientific literature is contradictory as illustrated by the following examples. The publications from Gloesmann et al.[32] and Slijkerman et al.[47] show figures with contradicting information regarding the

Table 1. Nomenclature of Outer Retinal Bands Visible on SD-OCT B-Scan Images in Humans (Adapted From Staurenghi et al.[12])

Reflectivity on SD-OCT	Name of Zone According to OCT Consensus[12]
Hyperreflective	External limiting membrane (ELM)
Hyporeflective	Myoid zone of the photoreceptors (MZ)
Hyperreflective	Ellipsoid zone of the photoreceptors (EZ)
Hyporeflective	Outer segments of the photoreceptors (OS)
Hyperreflective	Photoreceptor interdigitation with RPE (IZ)
Hyperreflective	RPE/BM complex (RPE/BM)
Thin layer of moderate reflectivity in inner choroid	Choriocapillaris (CC)

localization of the OS and RPE/BM zones in pigs. The publications from Muraoka et al.[30] and Bartuma et al.[48] disagree regarding labeling of the interdigitation zone (IZ), RPE zone, and BM zone in rabbits. In rats, the publications from Yamauchi et al.[21] and Lozano and Twa[22] show the RPE/BM zone in different localizations, whereas the publications from Hein et al.[24] and Hariri et al.[23] identify the same structure once as inner segment (IS) (combined myoid and ellipsoid zones [EZs]) and once as OS zone. In mice, the publication from Ferguson et al.[17] identifies a hyporeflective structure as RPE/BM, whereas Zam et al.[18] identify a hyperreflective structure as RPE/BM. Similar concerns regarding the completeness and consistency across research groups of layer and band designation and labeling nomenclature of mouse retinal OCTs were raised by DeRamus et al.[49]

We assume that these discrepancies are partially caused by the use of different OCT technologies, the rapid development of new OCT technologies with increased image resolution, and the changes in nomenclature during the years when the studies referenced earlier were published. Moreover, we believe that a direct, and possibly erroneous, translation of knowledge regarding ORB anatomy in humans to various animal species might have also facilitated such discrepancies. A direct application of human OCT layer definitions to animal OCTs might not be possible due to the fact that retinal anatomy varies across species as a result of differences in photoreceptor length and morphology, rod and cone ratios, or organelle distribution in the RPE.[50] Correct identification of the outer retinal margin is vital for repeatable retinal thickness measurements and proper identification of ORB on OCT images across species. In humans, the outermost hyperreflective layer, later confirmed to be the RPE/BM,[7] has been a reliable identifier of the outer retinal margin since the early days of OCT examinations.[51] However, choroidal structures can have similar or higher reflectivity than the RPE/BM in nonhuman species.[48,49,52] A direct translation to nonhuman species of the interpretation of the outermost hyperreflective layer as a reliable identifier of the outer retinal margin on OCT images of human subjects can therefore be unreliable. We believe that this has also been a major problem for autosegmentation algorithms in nonhuman species, making total retinal thickness measurements inaccurate.[52] In short, correct ORB and outer retinal margin identification is essential for reproducibility of research results, translation of animal data to humans and correlation of OCT and histology data.

Therefore, in this study, two questions were addressed. First, we hypothesized that the choriocapillaris and its connecting vasculature can be reliably identified across species as a hyporeflective band external to the RPE/BM complex and can thus be used as a reliable marker to define the outer retinal margin. We therefore quantified the percentage of OCT B-scans with an identifiable choriocapillaris band in the superior, central, and inferior retina in four common experimental animal species (minipig, rabbit, rat, mouse). OCT findings were correlated with histology. Second, we hypothesized that the presentation of ORB on OCT might vary across species on account of interspecies differences in retinal anatomy. We therefore defined the ideal presentation of ORB on best quality OCT images in the same anatomic locations across the same four animal species. The percentage of OCT B-scans with ideal ORB presentation was quantified.

Methods

The experimental preclinical testing protocols were approved by the Institutional Animal Care and Use Committee of the Cantonal Veterinary Office Basel, Basel, Switzerland. The animal facility is accredited by the Association for Assessment and Accreditation of Laboratory Animal Care International. All animals were treated in accordance with the guidelines of the ARVO Statement for the Use of Animals in Ophthalmic and Vision Research and the applicable Swiss regulations.

Animals

OCT B-scans of untreated control animals enrolled in various preclinical drug trials were retrieved from the OCT database at the Roche Innovation Center Basel. All animals underwent complete ophthalmic examinations including slit-lamp biomicroscopy, indirect ophthalmoscopy, and IOP measurement at baseline and before imaging. Animals were excluded from the trials if optical axis opacities were present at these time points.

Image Acquisition

All images were acquired with a Spectralis HRA+OCT combined confocal scanning laser ophthalmoscopy (cSLO) and SD-OCT system (Heidelberg Engineering, Heidelberg, Germany) equipped with a widefield 55° noncontact lens (Heidelberg Engineering). All imaging was performed between 8 AM and 1 PM with the animals under general anesthesia, induced and maintained using routine and approved protocols (Supplementary Table S1). The eyes were not dark adapted and were dilated with 0.5% tropicamide eye drops (Mydriaticum Stulln; Pharma Stulln GmbH, Stulln, Germany) on induction of anesthesia. The eyes were aligned with the Spectralis HRA+OCT instrument by positioning the optic nerve head (ONH) in the center of the cSLO image. All eyes were kept lubricated (Dynawell 3; Schalcon SpA, Rome, Italy), and hard contact lenses (Cantor+Nissel, Brackley, UK) were applied to the cornea in rodents to protect the cornea from desiccation and to reduce noise in the OCT images.

Horizontal B-scans were acquired from three anatomic locations as depicted in Figure 1: central scans through the optic disc and dorsal and ventral scans located one optic disc diameter distance dorsal and ventral from the optic disc border, respectively. The B-scans were oriented parallel to the long axis of the optic disc in rabbits and minipigs. Retinal layers are not visible on horizontal central position B-scans in rabbits because the rabbit has very thick and reflective medullary rays. Instead, a paracentral B-scan was acquired immediately ventral to the extension of the medullary rays as observed on cSLO images. All B-scans were acquired and evaluated in Spectralis software V6.9a (Heidelberg Engineering) and fulfilled the following criteria: 55° length, averaged over 40 B-scans or more, HR mode (high resolution), no enhanced depth imaging. The Spectralis system uses a signal-to-noise ratio (SNR) in decibels

Investigative Ophthalmology & Visual Science

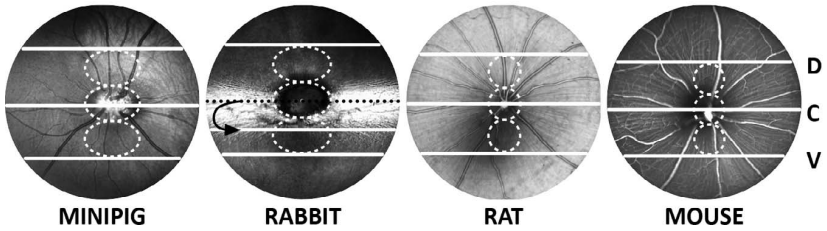

FIGURE 1. Methodology of SD-OCT B-scan acquisition in dorsal (D) central (C) and ventral (V) fundus locations across species. OCT B-scan localization illustrated on overview images of the normal fundus of a minipig, rabbit, rat, and mouse acquired via cSLO. All OCT B-scans were acquired in a horizontal plane. Central (C) scans were centered through the optic disc. Dorsal (D) and ventral (V) scans were located one optic disc diameter distance dorsal and ventral from the optic disc border, respectively. In rabbits, the thick and optically reflective medullary rays preclude the visualization of any retinal details in central section scans; therefore, paracentral B-scans located directly ventral to the extension of the medullary rays were acquired instead (*arrow*).

as internal instrument B-scan quality value. B-scans with an SNR ratio lower than 24 dB were excluded from the analyses to insure the use of best-quality images, as specified by the cSLO and SD-OCT system and Heyex software manufacturer and in previous publications.[53–56] A maximum number of 128 B-scans was evaluated per species/strain (minipigs, rabbits, pigmented and albino rats and pigmented and albino mice; details in Supplementary Table S2). Animals were included if both eyes could be examined, and at least four scans fulfilled the criteria specified above. Twelve additional B-scans from four cynomolgus monkeys were included to illustrate the nonhuman primate choriocapillaris for histology comparison purposes.

Image Evaluation and Statistics

B-scans were independently evaluated by two experienced OCT readers (PS, PM). First, the number of OCT B-scans on which a choriocapillaris layer could clearly be identified was determined per anatomic location and quantified as number of OCT B-scans with identifiable choriocapillaris layer per total number of OCT B-scans. The choriocapillaris was identified on OCT scans as the innermost narrow horizontal hyporeflective linear structure of the choroid with hyporeflective canals indicating vascular connections to the more externally located major choroidal vessels. Second, B-scans demonstrating the highest discernible number of individual ORB for a specific species were defined as ideal scan presentation for that particular species. The number of ideal presentation B-scans per total number of B-scans was determined, and different anatomic locations were compared per species. Differences in SNR quality of OCT B-scans between species were evaluated with a two-tailed Mann-Whitney *U* test. Influence of the pigmentation status of rats and mice on choriocapillaris layer identifiability and ORB discernibility was evaluated with a Pearson's χ^2 test. $P < 0.05$ was considered to represent a statistically significant difference between compared samples. The interrater agreement and discrepancies between OCT readers regarding choriocapillaris layer identifiability and ORB discernibility were statistically evaluated through Cohen's κ coefficient calculation with agreement indication according to Landis and Koch.[57,58]

Comparison of OCT B-Scan Findings to Histology

All the animals presented in this study were euthanized for reasons related to the original preclinical drug trials and were enrolled as healthy untreated or vehicle-treated controls. Clinical or imaging abnormalities were not observed in any of these animals. The enucleated eyes were immersed intact in Davidson solution (A3200; PanReac AppliChem, Darmstadt, Germany) for 48 hours and postfixed in 70% ethanol for 24 hours before dissection and standard automated dehydration and paraffin-embedding processing (Tissue-Tek VIP 5; Sakura, Alphen aan den Rijn, The Netherlands). The eyes were retrieved from the tissue archive at the Roche Innovation Center Basel. Four-micrometer-thick sections were cut at the locations of the OCT scan examinations and stained with hematoxylin-eosin. The slides were evaluated via bright-field microscopy and documented by CCD camera (Zeiss Axioscope A1 with C-Apochromat 63×/NA 1.20 W objective and Axiocam 305; Carl Zeiss, Feldbach, Switzerland). Histology served to verify the position of the choriocapillaris layer and the presence of vascular connections to the more externally located major choroidal vessel layer as identified on the OCT B-scans.

RESULTS

Overall, 574 B-scans from 96 subjects were evaluated. The SNR quality of the images from the minipigs (28.7), rabbits (29.6), and pigmented (29.3) and albino rats (29.4) was comparable ($P > 0.19$, Mann-Whitney *U* test). Compared with the other species examined, the SNR quality of the images from pigmented and albino mice was significantly higher (32.8, $P < 1E^{-5}$) and lower (26.1, $P < 1E^{-5}$), respectively. A narrow linear hyporeflective structure directly adjacent and external to and parallel with the hyperreflective RPE/BM complex was presumed to represent the choriocapillaris on OCT scans (Figs. 2A, 2B). Histology on the same minipig eye confirmed the presence of a choriocapillaris of similar thickness and identical anatomic localization (Figs. 2C, 2D). Vascular connections between the choriocapillaris and the more externally located major choroidal vessels could be localized on both OCT B-scans and histology sections in all species evaluated (Fig. 3). The choriocapillaris visibility and ideal ORB presentation results across species and strains are summarized in Figures 4 and 5, respectively. The ideal ORB presentation on SD-OCT B-scans is illustrated with longitudinal reflectivity profile for each species in Figure 6. A selection of SD-OCT B-scans including longitudinal reflectivity profiles with nonideal ORB presentation for each species is illustrated in Supplementary Figure S1. Interrater reliability κ statistics for the evaluation of choriocapillaris visibility and ORB presentation are summarized in Table 2.

Minipigs

One hundred twenty-eight B-scans from 20 animals (Göttingen Minipigs, Ellegaard, Denmark) were evaluated. The choriocapillaris was identifiable with perfect interrater reliability ($\kappa = 1$) on all B-scans. The ideal ORB presentation consisted of three hyperreflective bands (Fig. 6) and was identified on 11.7% of

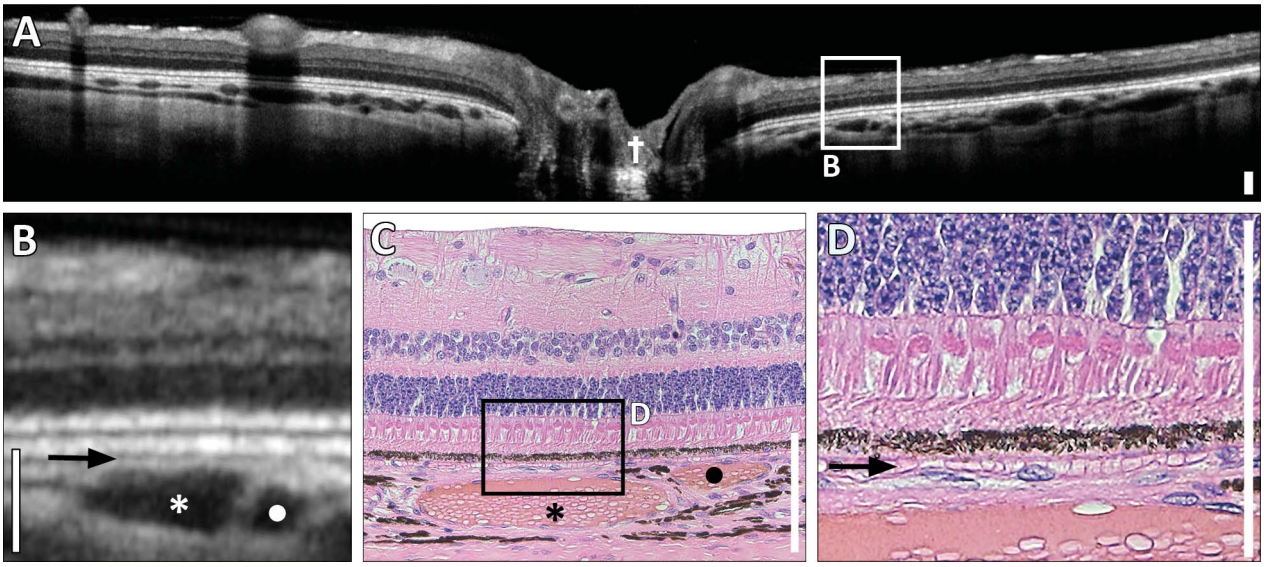

FIGURE 2. Correlation of SD-OCT and histology of minipig eye. (**A**) SD-OCT B-scan of the minipig retina passing through the optic nerve head (†) with details in a cut out (**B**) depicting two large choroidal vessels (*, •). A narrow linear hyporeflective structure directly adjacent and external to and parallel with the hyperreflective RPE/BM complex was presumed to be the choriocapillaris on this OCT scan (*arrow* in **B**). (**C**) Hematoxylin-eosin microphotograph of the corresponding area in the same eye. The cut out (**D**) depicts a single layer of erythrocytes representing the choriocapillaris (*arrow*) directly external to the RPE and Bruch's membrane. The same two large choroidal vessels are marked (*, •) in the SD-OCT scan (**B**) and histology image (**C**). Axial *scale bars*: 100 µm.

the B-scans (all absolute values included in Supplementary Table S2). There was a large location difference with most of the ideal scans identified at the dorsal location (27.9%) compared with the central (2.3%) and ventral (4.9%) locations. Two hyperreflective bands could be identified on most B-scans. The interrater reliability demonstrated an almost perfect agreement ($\kappa = 0.85$). Interestingly, a faint separation line was identified within the second hyperreflective band on five B-scans with ideal ORB presentation (Fig. 6).

Rabbits

Sixty-five B-scans from 12 rabbits (Dutch-belted Pigmented Rabbits; Covance, Denver, CO, USA) were evaluated. The choriocapillaris layer was identifiable on 70.8% of B-scans. A large difference between dorsal, paracentral, and ventral locations was observed with the choriocapillaris layer identifiable on 17.4%, 100%, and 100% of the B-scans, respectively. The ideal ORB presentation consisted of three hyperreflective bands (Fig. 6) and was identified on 73.8% of the scans. Most of the ideal ORB presentation scans were in the paracentral (100%) and ventral locations (92.1%) compared with the dorsal location (32.6%). The hyporeflective band between the second and third hyperreflective bands appeared thickened in the paracentral and ventral locations compared with the dorsal location. The interrater reliability for both visibility of choriocapillaris ($\kappa = 0.93$) and ideal ORB presentation ($\kappa = 0.92$) indicated almost perfect agreement.

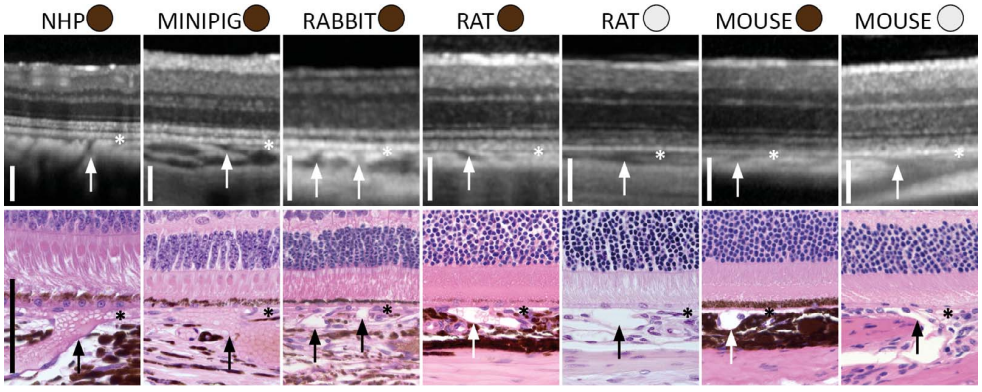

FIGURE 3. Localization of the choriocapillaris and connecting vasculature across common laboratory animal species. The choriocapillaris is marked in all SD-OCT B-scans and histology images with *asterisks* and the connecting vasculature, precapillary arterioles and postcapillary venules, with *arrows*. On histology specimens, these vascular structures were more readily visible in eyes that were not completely bled out (NHP, nonhuman primate; minipig). No difference was observed between pigmented and albino rodent strains regarding the shape of the connecting vasculature. Pigmented strain/species marked with *brown circles*; albino strain/species with *gray circles*. Axial *scale bars*: 100 µm. Microscopy *scale bar* applies to all histology images.

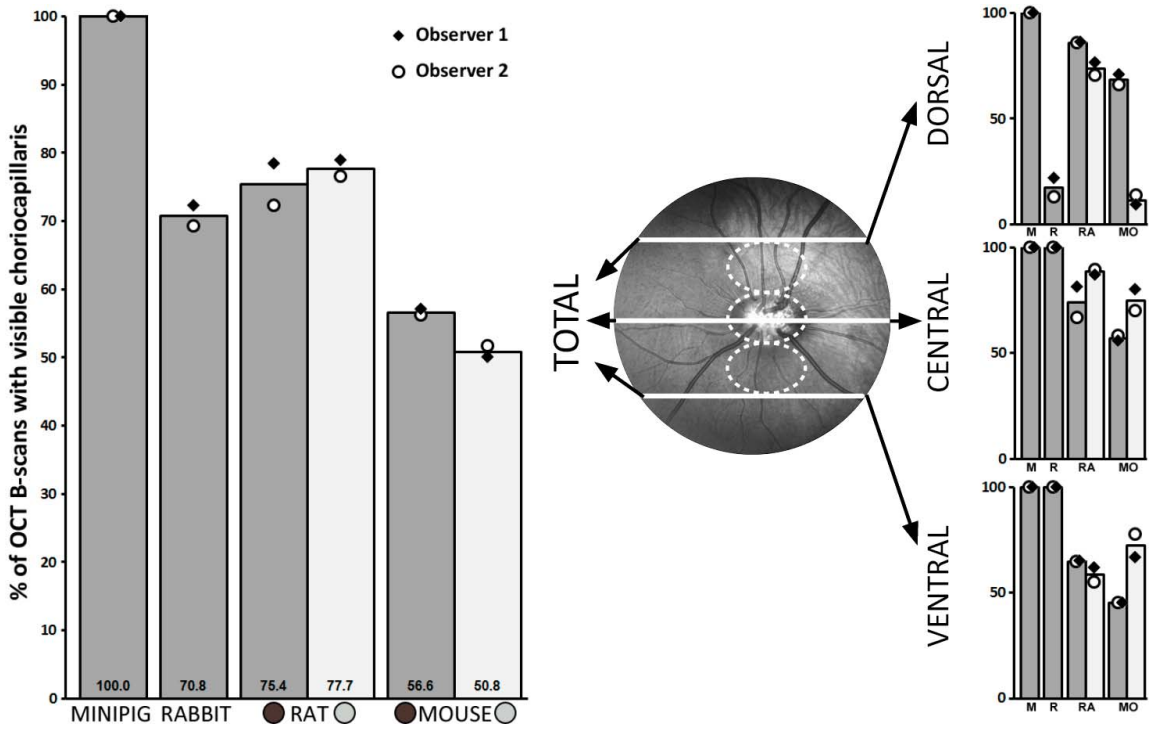

FIGURE 4. Visibility of the choriocapillaris across common laboratory animal species. Percentage of B-scans across species and strains in which the choriocapillaris and connecting vasculature were visible. The bar chart on the *left* depicts the averages across the three scan locations per species and strain for both observers. The bar charts on the *right* show the distribution across the three scan locations. All values included in Supplementary Table S2.

Rats

One hundred ninety-three rat retina B-scans were evaluated, of which 65 were from pigmented rats ($n = 9$) (Brown-Norway; Charles River, Sulzfeld, Germany) and 128 from albino rats ($n = 24$) (Wistar [Han9]; Charles River). The choriocapillaris was identifiable on 75.4% of pigmented rat and 77.7% of albino rat B-scans with no significant difference between strains ($P_{Observer1} = 0.94$, $P_{Observer2} = 0.52$, Pearson's χ^2). There were some differences across the B-scan locations. The choriocapillaris was visible on 85.7% of dorsal, 74.1% of central, and 64.7% of ventral location B-scans from pigmented rats, whereas albino rats had a visible choriocapillaris on 73.5% of dorsal, 88.5% of central, and 58.6% of ventral B-scans. The ideal ORB presentation consisted of four hyperreflective bands (Fig. 6) and was observed on 80.0% of pigmented rat B-scans compared with 28.5% of albino rat B-scans, which was a highly significant difference for both observers ($P_{Observer1} < 1E^{-5}$, $P_{Observer2} < 1E^{-5}$; Pearson's χ^2). Differences in ideal ORB presentation across locations were observed in pigmented (85.7% dorsal, 74.1% central, and 82.4% ventral) and in albino rats (32.4% dorsal, 32.3% central, and 15.5% ventral). The interrater reliability for choriocapillaris visibility ($\kappa_{pigmented} = 0.75$, $\kappa_{albino} = 0.71$) indicated substantial agreement between OCT scan readers, whereas the interrater reliability for ideal ORB presentation ($\kappa_{pigmented} = 0.90$, $\kappa_{albino} = 0.87$) indicated almost perfect agreement.

Mice

One hundred eighty-eight mouse retina B-scans were evaluated, of which 128 were from pigmented mice ($n = 21$) (C57BL/6; Charles River) and 60 from albino mice ($n = 10$) (NMRI [Han]; Charles River). The choriocapillaris was identifiable on 56.5% of pigmented mouse and 50.8% of albino mouse B-scans with no significant difference between the strains ($P_{Observer1} = 0.37$, $P_{Observer2} = 0.56$, Pearson's χ^2). Large differences in choriocapillaris visibility were observed across B-scan locations. The choriocapillaris was visible on 68.3% of dorsal, 57.0% of central, and 45.5% of ventral location B-scans from pigmented mice, whereas albino mice had a visible choriocapillaris on 11.4% of dorsal, 75.0% of central, and 72.2% of ventral location B-scans. The ideal ORB presentation consisted of four hyperreflective bands (Fig. 6) and was observed on 91.0% of pigmented mouse B-scans compared with 62.5% of albino mouse B-scans, which was a highly significant difference for both observers ($P_{Observer1} < 1\ E^{-5}$, $P_{Observer2} < 1\ E^{-5}$, Pearson's χ^2). Differences in ideal ORB presentation were observed across locations in pigmented (79.3% dorsal, 97.7% central, and 95.5% ventral) and albino mice (50.0% dorsal, 85.0% central, and 52.8% ventral). The interrater reliability for choriocapillaris visibility indicated substantial agreement ($\kappa_{pigmented} = 0.77$) and almost perfect agreement ($\kappa_{albino} = 0.86$) between OCT scan readers for pigmented and albino animals, respectively. The interrater reliability for ideal ORB presentation ($\kappa_{pigmented} = 0.95$, $\kappa_{albino} = 0.82$) indicated an almost perfect agreement between OCT scan readers for both strains.

DISCUSSION

Although OCT has become the standard in retinal imaging, the controversy regarding qualification of the ORB that can be distinguished on OCT scans in humans is ongoing.[6–8] Likewise, many published OCT studies conducted with animals demonstrate that uniformity in ORB identification is not self-evident.[17,18,21–24,30,32,47–49] In this context, our study shows

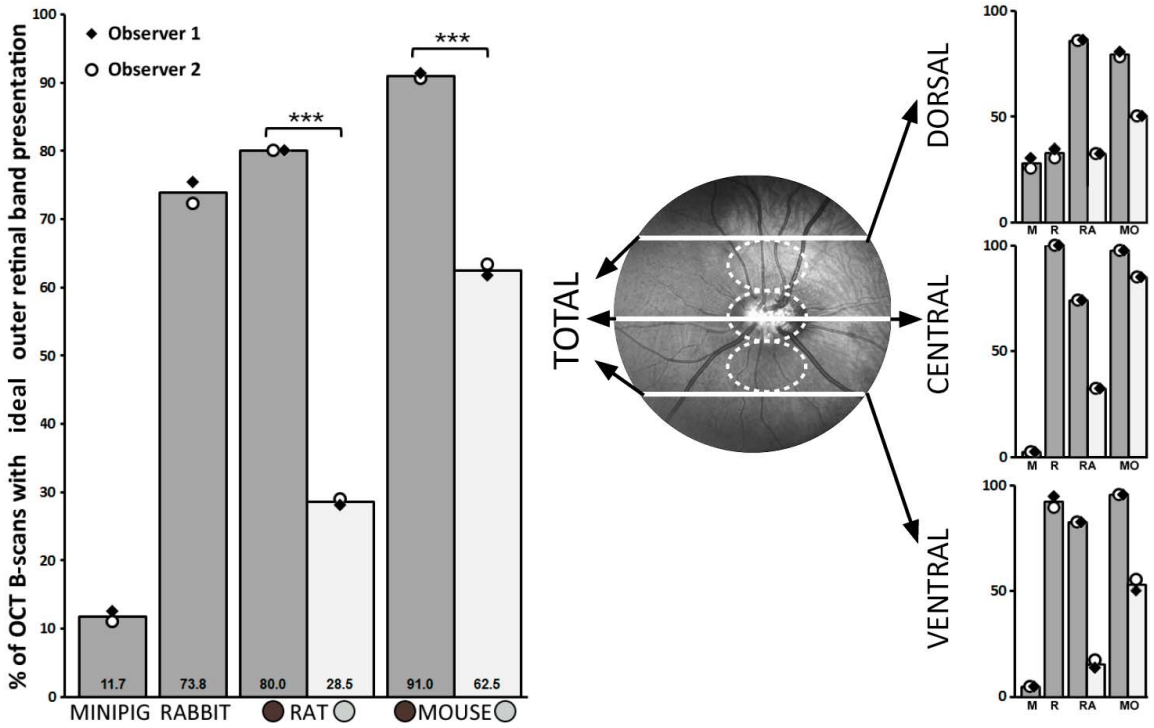

Figure 5. Ideal outer retinal band presentation across common laboratory animal species**.** Percentage of B-scans across species and strains in which the ideal outer retinal band presentation for that particular species could be identified. The bar chart on the *left* depicts the averages across the three scan locations per species and strain for both observers. The bar charts on the *right* show the distribution across the three scan locations. Statistically significant differences between pigmented and nonpigmented strains are marked with *asterisks*. All values included in Supplementary Table S2.

that the choriocapillaris layer was a reliable marker of the outer retinal margin on most OCT scans across species. This study also documented the ideal presentation of ORB for the animal species evaluated. Also, the percentage of OCT B-scans with ideal ORB presentation was highest in areas of retinal specialization in minipigs (area centralis) and rabbits (visual streak), whereas no distinct pattern in ideal ORB presentation distribution was recognized in animals without areas of retinal specialization (rats and mice).

Our OCT–histology comparisons demonstrate that the choriocapillaris is likely best defined on OCT as a linear hyporeflective space directly external to the RPE/BM complex and not as a diffusely defined, hyperreflective band interior to the large choroidal vessel layer, as previously suggested.[48]

Bartuma et al. stated that the choriocapillaris is often difficult to separate from the RPE/BM complex on OCT B-scans in rabbits.[48] In our study, this was true only for the OCT B-scans acquired from the scan location dorsal to the ONH. The choriocapillaris and connecting arterioles could be identified on every OCT B-scan acquired from the paracentral and ventral locations. The obvious difference in choriocapillaris and connecting vasculature visibility between dorsal and paracentral/ventral OCT B-scans in rabbits is probably the result of better detail resolution on the ventral OCT B-scans. These OCT B-scans originate from the rabbit visual streak, which is located ventral to the ONH.[59]

Despite the absence of a statistical difference in choriocapillaris visibility between pigmented and albino rodents, both OCT observers had the distinct impression that the identification of the connecting vasculature was more difficult in albino than in pigmented strains, which is most likely caused by lack of pigment in choroidal structures. A similar conclusion was reached by Berger et al., who reported better visibility of the choriocapillaris in pigmented mice and less defined choroidal structures in albino mice.[60] The evaluation of serial B-scans or true volume scans instead of single line scans might increase the likelihood of identifying the connecting vasculature and choriocapillaris, thus improving the value of the choriocapillaris as marker for identification of the outer retinal margin in mice.

The ideal ORB presentation on OCT B-scans in minipigs and rabbits consisted of three hyperreflective bands, considered to be the ELM, EZ, and combined IZ with RPE/BM complex. In minipigs, the visibility of all three ORBs was best in the dorsal scan location. We hypothesize that this is most likely due to the fact that the porcine area centralis, where the photoreceptor cells are most tightly packed and the cone density is highest, is located dorsal to the ONH.[61–63] The visibility of all three ORBs was best in the visual streak at the ventral scan location in rabbits.[59,64] The rabbit visual streak has cone and total photoreceptor density features comparable with the minipig area centralis.[64,65] The visual streak origin of the paracentral and ventral OCT B-scans in rabbits is further supported by the observed thickening of the photoreceptor OS layer (the hyporeflective band between the second and third hyperreflective bands) on these scans as confirmed via histology.[66] Although many papers have been published on rabbit retinal topography, most of the publications are focused on ganglion cell or cone flat-mount densities.[59,64,65,67] In the figures included in some publications, one can recognize that the photoreceptor outer segments are longest in the visual streak in wild-type rabbits (figure 4C in Ref. 68). A difference in photoreceptor anatomy between long and thin central foveal cones and shorter, thicker perifoveal cones in humans was

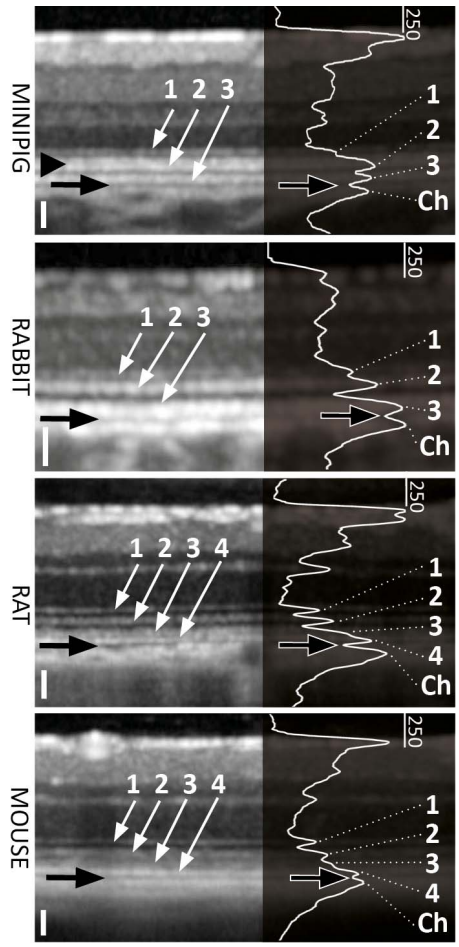

Figure 6. Ideal outer retinal band presentation on SD-OCT B-scans. The ideal outer retinal band presentation in minipigs and rabbits was with three hyperreflective outer retinal bands, presumably representing the ELM (1), EZ (2), and combined IZ and RPE/BM (3). The ideal outer retinal band presentation in all rodents was with four hyperreflective outer retinal bands, presumably representing the ELM (1), EZ (2), IZ (3), and RPE/BM (4). *Black arrows* indicate the choriocapillaris in both OCT and reflectivity profile images. A dip in reflectivity representing the choriocapillaris between the hyperreflectivity peaks in the proximal choroid (Ch) and RPE/BM is a noteworthy observation on the reflectivity profiles in all species. Also, the proximal choroid displays similar or increased reflectivity compared with the RPE/BM. The *black arrowhead* indicates a faint separation line within the second hyperreflective band as observed on a number of minipig OCTs. OCT location and SNR: minipig: dorsal, 30; rabbit: ventral, 29; rat pigmented: dorsal, 33; mouse pigmented: ventral, 29. Axial *scale bars*: 50 μm.

reviewed by Spaide and Curcio in 2011 and thought to explain differences in ORB presentation and thickness on OCT between the fovea and perifovea.[7] We hypothesize that differences in ORB presentation and photoreceptor OS layer thickness on OCT between regions within and outside of the visual streak in rabbits and minipigs might be explained by similar differences in photoreceptor anatomy. However, to the best of our knowledge, this cannot be confirmed because no publications comparing photoreceptor anatomy on cross section in various regions of the retina exist for rabbits or minipigs.

Based on Figure 5, there does not seem to be a consistent pattern to the observed differences in ORB presentation that might be explained by general differences in photoreceptor density, type, and morphology between retinal regions in rodents. Moreover, mice and rats do not have macula or area centralis-like regions of retinal specialization with corresponding specialized photoreceptor anatomy as present in primates and certain other animals.[69] Significant differences in photoreceptor density and anatomy between the central and peripheral retina do exist in mice[70] but cannot explain the differences in ORB presentation in our study, which were observed between various central retinal regions.

The ELM was the ORB with the worst visibility of the three ORB identified in minipigs, which supports the observation by Gloesmann et al. that the ELM was poorly visible and thought to coalesce with the myoid zone on OCT B-scans.[32] Interestingly, a faint splitting of the second hyperreflective ORB (EZ) by a very fine band of moderate reflectivity was observed on five minipig B-scans in the present study, but not in any of the other species. The authors believe that this was not an artifact, but also do not believe that this should be considered as the expected fourth ORB, as recognized on OCT scans of humans. If considered to be an actual fourth ORB, it would likely be considered the band corresponding to the IZ band, which would leave almost no space for the photoreceptor outer segments between EZ and IZ and a very large space that cannot be anatomically explained between IZ and RPE/BM. The authors rather hypothesize that the ultrastructural anatomy of the porcine rod and cone IS might be the source of the observed EZ splitting. The EZ band was hypothesized to arise from the ellipsoid zone of the photoreceptor IS in humans.[7,71] The ellipsoid portions of the rod and cone IS are located at the same level or largely overlap in humans, nonhuman primates,[72] sheep,[50] and mice.[73] However, ultrastructural study in swine retinas have demonstrated that the ellipsoid portion of the cone IS lies at the level of the rod myoid, whereas the ellipsoid portion of the rod IS is located more externally,[74] which could lead to the observed ORB splitting on OCT. Because all tissues of the animals included in this study were Davidson fixed and paraffin embedded, no ultrastructural investigations could be performed to test this hypothesis.

For all rodent strains, the ideal ORB presentation consisted of four hyperreflective bands, presumably of the same origin as the four hyperreflective bands of the outer retina in humans,[60,75] and is consistent with a proposed nomenclature

Table 2. Interrater Agreement κ Statistics

	Choriocapillaris Visibility		Outer Retinal Bands Presentation	
Species	κ	Agreement Indication	κ	Agreement Indication
Minipigs	1.00	Perfect	0.85	Almost perfect
Rabbits	0.93	Almost perfect	0.92	Almost perfect
Rats pigmented	0.75	Substantial	0.90	Almost perfect
Rats albino	0.71	Substantial	0.87	Almost perfect
Mice pigmented	0.77	Substantial	0.95	Almost perfect
Mice albino	0.86	Almost perfect	0.82	Almost perfect

for murine OCTs.[49] ORB presentation was significantly improved by the presence of melanin pigment in rodents in our study. Melanin granules (melanosomes) were found to be a primary source of reflectivity on OCT[76] and presence of melanin affects ORB appearance and reflectivity.[77]

All OCT B-scans evaluated in this study were acquired with a Spectralis HRA+OCT system, which is important to note because the design and processing algorithms of the OCT system have a large impact on final OCT B-scan quality.[78] The current study's results and conclusions are thus valid only for data generated with a Spectralis HRA+OCT system, which is still useful on a broad scale because the Spectralis HRA+OCT system is one of the most widely used OCT units on the market. However, choriocapillaris and connecting vasculature visibility and ORB discernibility might be different on OCT B-scans generated with OCT systems from different manufacturers. For example, Tian et al. were able to separately identify the IZ and RPE/BM bands on OCT B-scans generated by a custom-built OCT system in rabbits.[79] Moreover, the use of swept-source OCT technology offers reduced sensitivity roll-off with increased imaging depth. This results in a higher imaging range and better visualization of choroidal structures, which could improve choriocapillaris and connecting vasculature visibility.[80] Recent advances and increased clinical use of OCT angiography (OCTA)[81,82] brings the prospect of better choriocapillaris and connecting vasculature delineation. Although several papers on retinal OCTA exist,[83–85] to the best of our knowledge, no detailed literature focusing on OCTA of the choriocapillaris is available for the species covered in this paper.

Agreement for choriocapillaris visibility and ORB presentation between the two observers was substantial to high in all species, underlining the reproducibility and reliability of OCT B-scan scoring and serving as internal quality control. Longitudinal reflectivity profiles were not used as an objective end point evaluation tool for the whole dataset to reflect clinical reality of image display, grading, and interpretation under daily routine conditions. Furthermore, longitudinal reflectivity profiles also depend on image quality and threshold and can only be generated from single or several A-scans at a time, which introduces selection bias. Also, for some species, the thickness of different bands varies considerably within a single B-scan, and the tuning and averaging of the longitudinal reflectivity profiles over the whole scan range would theoretically be possible, but only with excessive effort.

All of the OCT B-scans evaluated in this study were acquired from animal species that lack a tapetum lucidum, a specialized inner choroidal structure that reflects light back toward and through the retina.[50,86] The reflective nature of the tapetum lucidum might interfere with choriocapillaris and connecting vasculature visibility and ORB discernibility. Similar future studies in tapetal species including cats and dogs[86] are needed to determine whether the results and conclusions of the current study also apply to tapetal species of interest to comparative vision scientists and veterinary ophthalmologists.

In conclusion, the choriocapillaris and its connecting vasculature are easy and valid markers for identification of the outer retinal border in minipigs, rabbits, rats, and mice. The value of these markers is proportionate to their visibility in individual B-scans (Fig. 4) and could potentially be increased via acquisition and evaluation of more consecutive serial or volume B-scans, especially in mice. Ideal ORB presentation in minipigs was low, with inconsistent visualization of the ELM, which makes identification of ORB from the choriocapillaris side inward a more valid approach than searching for the ELM in swine. Ideal ORB presentation was best in the area centralis and the visual streak area of minipigs and rabbits, respectively. Ideal ORB presentation was higher in pigmented mice and rats compared with albino mice and rats. Proper and consistent outer retinal margin and ORB identification are essential for reproducibility and translation of research results. As such, the observed differences in choriocapillaris visibility and ORB presentation between species, strains, and anatomic locations need to be taken into account when performing qualitative and quantitative OCT evaluations in comparative ophthalmic research.

Acknowledgments

The authors thank Lucienne Goetz, Martin Freiermuth, Michael Siegrist, Silvan Aegerter, Claudia Stutz, Nora Denk, and Christelle Zundel for technical support and Solveig Badillo for statistical advice.

Disclosure: **P. Soukup**, F. Hoffman La-Roche Ltd. (E); **P. Maloca**, F. Hoffman La-Roche Ltd. (C); **B. Altmann**, F. Hoffman La-Roche Ltd. (E); **M. Festag**, F. Hoffman La-Roche Ltd. (E); **E.-A. Atzpodien**, F. Hoffman La-Roche Ltd. (E); **S. Pot**, None

References

1. Gabriele ML, Wollstein G, Ishikawa H, et al. Optical coherence tomography: history, current status, and laboratory work. *Invest Ophthalmol Vis Sci*. 2011;52:2425–2436.
2. Marschall S, Sander B, Mogensen M, Jorgensen TM, Andersen PE. Optical coherence tomography-current technology and applications in clinical and biomedical research. *Anal Bioanal Chem*. 2011;400:2699–2720.
3. McLellan GJ, Rasmussen CA. Optical coherence tomography for the evaluation of retinal and optic nerve morphology in animal subjects: practical considerations. *Vet Ophthalmol*. 2012;15(suppl 2):13–28.
4. Hernandez-Merino E, Kecova H, Jacobson SJ, Hamouche KN, Nzokwe RN, Grozdanic SD. Spectral domain optical coherence tomography (SD-OCT) assessment of the healthy female canine retina and optic nerve. *Vet Ophthalmol*. 2011;14:400–405.
5. Srinivasan VJ, Monson BK, Wojtkowski M, et al. Characterization of outer retinal morphology with high-speed, ultrahigh-resolution optical coherence tomography. *Invest Ophthalmol Vis Sci*. 2008;49:1571–1579.
6. Jonnal RS, Kocaoglu OP, Zawadzki RJ, Lee S-H, Werner JS, Miller DT. The cellular origins of the outer retinal bands in optical coherence tomography images. *Invest Ophthalmol Vis Sci*. 2014;55:7904–7918.
7. Spaide RF, Curcio CA. Anatomical correlates to the bands seen in the outer retina by optical coherence tomography: literature review and model. *Retina*. 2011;31:1609–1619.
8. Cuenca N, Ortuño-Lizarán I, Pinilla I. Cellular characterization of OCT and outer retinal bands using specific immunohistochemistry markers and clinical implications. *Ophthalmology*. 2018;125:407–422.
9. Spaide RF. Outer retinal bands. *Invest Ophthalmol Vis Sci*. 2015;56:2505–2506.
10. Spaide RF. Questioning optical coherence tomography. *Ophthalmology*. 2012;119:2203–2204.
11. Curcio CA, Sparrow JR, Bonilha VL, Pollreisz A, Lujan BJ. Re: Cuenca et al.: cellular characterization of OCT and outer retinal bands using specific immunohistochemistry markers and clinical implications. *Ophthalmology*. 2018;125:e47–e48.
12. Staurenghi G, Sadda S, Chakravarthy U, Spaide RF. Proposed lexicon for anatomic landmarks in normal posterior segment spectral-domain optical coherence tomography: the IN•OCT consensus. *Ophthalmology*. 2014;121:1572–1578.
13. Saxena S, Srivastav K, Cheung CM, Ng JYW, Lai TYY. Photoreceptor inner segment ellipsoid band integrity on

spectral domain optical coherence tomography. *Clin Ophthalmol*. 2014;8:2507–2522.
14. Oishi A, Shimozono M, Mandai M, Hata M, Nishida A, Kurimoto Y. Recovery of photoreceptor outer segments after anti-VEGF therapy for age-related macular degeneration. *Graefes Arch Clin Exp Ophthalmol*. 2013;251:435–440.
15. Gharbiya M, Grandinetti F, Scavella V, et al. Correlation between spectral-domain optical coherence tomography findings and visual outcome after primary rhegmatogenous retinal detachment repair. *Retina*. 2012;32:43–53.
16. Witkin AJ, Ko TH, Fujimoto JG, et al. Ultra-high resolution optical coherence tomography assessment of photoreceptors in retinitis pigmentosa and related diseases. *Am J Ophthalmol*. 2006;142:945–952.
17. Ferguson LR, Balaiya S, Grover S, Chalam KV. Modified protocol for in vivo imaging of wild-type mouse retina with customized miniature spectral domain optical coherence tomography (SD-OCT) device. *Biol Proced Online*. 2012;14:9.
18. Zam A, Zhang P, Levine E, Pugh EN, Burns M, Zawadzki RJ. Evaluation of OCT for quantitative in-vivo measurements of changes in neural tissue scattering in longitudinal studies of retinal degeneration in mice. *Proc SPIE*. 2014;8934:893422.
19. Fischer MD, Huber G, Beck SC, et al. Noninvasive, in vivo assessment of mouse retinal structure using optical coherence tomography. *PLoS One*. 2009;4:e7507.
20. Huber G, Beck SC, Grimm C, et al. Spectral domain optical coherence tomography in mouse models of retinal degeneration. *Invest Ophthalmol Vis Sci*. 2009;50:5888–5895.
21. Yamauchi Y, Kimura K, Agawa T, et al. Correlation between high-resolution optical coherence tomography (OCT) images and histopathology in an N-methyl-N-nitrosourea–induced retinal degeneration rat model. *Br J Ophthalmol*. 2011;95:1161–1165.
22. Lozano DC, Twa MD. Quantitative evaluation of factors influencing the repeatability of SD-OCT thickness measurements in the rat. *Invest Ophthalmol Vis Sci*. 2012;53:8378–8385.
23. Hariri S, Tam MC, Lee D, Hileeto D, Moayed AA, Bizheva K. Noninvasive imaging of the early effect of sodium iodate toxicity in a rat model of outer retina degeneration with spectral domain optical coherence tomography. *J Biomed Opt*. 2013;18:26017.
24. Hein K, Gadjanski I, Kretzschmar B, et al. An optical coherence tomography study on degeneration of retinal nerve fiber layer in rats with autoimmune optic neuritis. *Invest Ophthalmol Vis Sci*. 2012;53:157–163.
25. Anger EM, Unterhuber A, Hermann B, et al. Ultrahigh resolution optical coherence tomography of the monkey fovea. Identification of retinal sublayers by correlation with semithin histology sections. *Exp Eye Res*. 2004;78:1117–1125.
26. Fortune B, Hardin C, Reynaud J, et al. Comparing optic nerve head rim width, rim area, and peripapillary retinal nerve fiber layer thickness to axon count in experimental GlaucomaS-DOCT parameters relationships to axon counts. *Invest Ophthalmol Vis Sci*. 2016;57:OCT404–OCT412.
27. Strouthidis NG, Fortune B, Yang H, Sigal IA, Burgoyne CF. Longitudinal change detected by spectral domain optical coherence tomography in the optic nerve head and peripapillary retina in experimental glaucoma. *Invest Ophthalmol Vis Sci*. 2011;52:1206–1219.
28. Arana LA, Pinto AT, Chader GJ, et al. Fluorescein angiography, optical coherence tomography, and histopathologic findings in a VEGF165 animal model of retinal angiogenesis. *Graefes Arch Clin Exp Ophthalmol*. 2012;250:1421–1428.
29. Koinzer S, Saeger M, Hesse C, et al. Correlation with OCT and histology of photocoagulation lesions in patients and rabbits. *Acta Ophthalmologica*. 2013;91:e603–e611.
30. Muraoka Y, Ikeda HO, Nakano N, et al. Real-time imaging of rabbit retina with retinal degeneration by using spectral-domain optical coherence tomography. *PLoS One*. 2012;7:e36135.
31. Yamauchi Y, Agawa T, Tsukahara R, et al. Correlation between high-resolution optical coherence tomography (OCT) images and histopathology in an iodoacetic acid-induced model of retinal degeneration in rabbits. *Br J Ophthalmol*. 2011;95:1157–1160.
32. Gloesmann M, Hermann B, Schubert C, Sattmann H, Ahnelt PK, Drexler W. Histologic correlation of pig retina radial stratification with ultrahigh-resolution optical coherence tomography. *Invest Ophthalmol Vis Sci*. 2003;44:1696–1703.
33. Fatehee N, Yu PK, Morgan WH, Cringle SJ, Yu DY. Correlating morphometric parameters of the porcine optic nerve head in spectral domain optical coherence tomography with histological sections. *Br J Ophthalmol*. 2011;95:585–589.
34. Atzpodien EA, Jacobsen B, Funk J, et al. Advanced clinical imaging and tissue-based biomarkers of the eye for toxicology studies in minipigs. *Toxicol Pathol*. 2016;44:398–413.
35. He Y, Sun Y, Chen M, et al. Automatic segmentation of canine retinal OCT using adaptive gradient enhancement and region growing. *Proc SPIE*. 2016:9788:978871Q.
36. Schallek JB, McLellan GJ, Viswanathan S, Ts'o DY. Retinal intrinsic optical signals in a cat model of primary congenital glaucoma. *Invest Ophthalmol Vis Sci*. 2012;53:1971–1981.
37. Beltran WA, Cideciyan AV, Guziewicz KE, et al. Canine retina has a primate fovea-like bouquet of cone photoreceptors which is affected by inherited macular degenerations. *PLoS One*. 2014;9:e90390.
38. Antony BJ, Abramoff MD, Harper MM, et al. A combined machine-learning and graph-based framework for the segmentation of retinal surfaces in SD-OCT volumes. *Biomed Opt Express*. 2013;4:2712–2728.
39. Abbott CJ, McBrien NA, Grünert U, Pianta MJ. Relationship of the optical coherence tomography signal to underlying retinal histology in the tree shrew (*Tupaia belangeri*). *Invest Ophthalmol Vis Sci*. 2009;50:414–423.
40. Huber G, Heynen S, Imsand C, et al. Novel rodent models for macular research. *PLoS One*. 2010;5:e13403.
41. Sajdak BS, Bell BA, Lewis TR, et al. Assessment of outer retinal remodeling in the hibernating 13-lined ground squirrel. *Invest Ophthalmol Vis Sci*. 2018;59:2538–2547.
42. Lu R-W, Curcio CA, Zhang Y, et al. Investigation of the hyperreflective inner/outer segment band in optical coherence tomography of living frog retina. *J Biomed Optics*. 2012;17:060504.
43. Zhang Q, Lu R, Wang B, Messinger JD, Curcio CA, Yao X. Functional optical coherence tomography enables in vivo physiological assessment of retinal rod and cone photoreceptors. *Sci Rep*. 2015;5:9595.
44. Tam BM, Moritz OL. Dark rearing rescues P23H rhodopsin-induced retinal degeneration in a transgenic *Xenopus laevis* model of retinitis pigmentosa: a chromophore-dependent mechanism characterized by production of N-terminally truncated mutant rhodopsin. *J Neurosci*. 2007;27:9043–9053.
45. Bell BA, Yuan A, Dicicco RM, Fogerty J, Lessieur EM, Perkins BD. The adult zebrafish retina: in vivo optical sectioning with confocal scanning laser ophthalmoscopy and spectral-domain optical coherence tomography. *Exp Eye Res*. 2016;153:65–78.
46. Bailey TJ, Davis DH, Vance JE, Hyde DR. Spectral-domain optical coherence tomography as a noninvasive method to assess damaged and regenerating adult zebrafish retinas SD-OCT of light-damaged zebrafish retinas. *Invest Ophthalmol Vis Sci*. 2012;53:3126–3138.
47. Slijkerman RWN, Song F, Astuti GDN, et al. The pros and cons of vertebrate animal models for functional and therapeutic

research on inherited retinal dystrophies. *Prog Retin Eye Res*. 2015;48:137–159.

48. Bartuma H, Petrus-Reurer S, Aronsson M, Westman S, André H, Kvanta A. In vivo imaging of subretinal bleb-induced outer retinal degeneration in the rabbit subretinal bleb-induced retinal degeneration. *Invest Ophthalmol Vis Sci*. 2015;56: 2423–2430.
49. DeRamus ML, Stacks DA, Zhang Y, Huisingh CE, McGwin G, Pittler SJ. GARP2 accelerates retinal degeneration in rod cGMP-gated cation channel beta-subunit knockout mice. *Sci Rep*. 2017;7:42545.
50. Samuelson DA. Ophthalmic anatomy. In: Gelatt KN, Gilger BC, Kern TJ, eds. *Veterinary Ophthalmology*. Ames, IA: Wiley-Blackwell; 2013:39–170.
51. Hee MR, Puliafito CA, Wong C, et al. Optical coherence tomography of macular holes. *Ophthalmology*. 1995;102: 748–756.
52. Dysli C, Enzmann V, Sznitman R, Zinkernagel MS. Quantitative analysis of mouse retinal layers using automated segmentation of spectral domain optical coherence tomography images algorithms for segmentation of murine retina. *Trans Vis Sci Tech*. 2015;4(4):9.
53. Leite MT, Rao HL, Zangwill LM, Weinreb RN, Medeiros FA. Comparison of the diagnostic accuracies of Spectralis, Cirrus and RTVue optical coherence tomography devices in glaucoma. *Ophthalmology*. 2011;118:1334–1339.
54. Balasubramanian M, Bowd C, Vizzeri G, Weinreb RN, Zangwill LM. Effect of image quality on tissue thickness measurements obtained with spectral-domain optical coherence tomography. *Optics Express*. 2009;17:4019–4036.
55. Faghihi H, Hajizadeh F, Hashemi H, Khabazkhoob M. Agreement of two different spectral domain optical coherence tomography instruments for retinal nerve fiber layer measurements. *J Ophthalmic Vis Res*. 2014;9:31–37.
56. Grover S, Murthy RK, Brar VS, Chalam KV. Comparison of retinal thickness in normal eyes using Stratus and Spectralis optical coherence tomography. *Invest Ophthalmol Vis Sci*. 2010;51:2644–2647.
57. Landis JR, Koch GG. The measurement of observer agreement for categorical data. *Biometrics*. 1977;33:159–174.
58. Burn CC, Weir AAS. Using prevalence indices to aid interpretation and comparison of agreement ratings between two or more observers. *Vet J*. 2011;188:166–170.
59. Vaney DI. A quantitative comparison between the ganglion cell populations and axonal outflows of the visual streak and periphery of the rabbit retina. *J Comp Neurol*. 1980;189:215–233.
60. Berger A, Cavallero S, Dominguez E, et al. Spectral-domain optical coherence tomography of the rodent eye: highlighting layers of the outer retina using signal averaging and comparison with histology. *PLoS One*. 2014;9:e96494.
61. Chandler MJ, Smith PJ, Samuelson DA, MacKay EO. Photoreceptor density of the domestic pig retina. *Vet Ophthalmol*. 1999;2:179–184.
62. Garcia M, Ruiz-Ederra J, Hernandez-Barbachano H, Vecino E. Topography of pig retinal ganglion cells. *J Comp Neurol*. 2005;486:361–372.
63. Hendrickson A, Hicks D. Distribution and density of medium- and short-wavelength selective cones in the domestic pig retina. *Exp Eye Res*. 2002;74:435–444.
64. Famiglietti EV, Sharpe SJ. Regional topography of rod and immunocytochemically characterized "blue" and "green" cone photoreceptors in rabbit retina. *Vis Neurosci*. 1995;12: 1151–1175.
65. Juliusson B, Bergström A, Röhlich P, Ehinger B, van Veen T, Szél A. Complementary cone fields of the rabbit retina. *Invest Ophthalmol Vis Sci*. 1994;35:811–818.
66. Lavaud A, Soukup P, Voelter K, Hartnack S, Pot SA. SD-OCT and histologic evaluation of the visual streak in experimental rabbits. In: Abstracts: the 49th Annual scientific meeting of the American college of veterinary ophthalmologists, Minneapolis, Minnesota, Sept 26–29, 2018. *Vet Ophthalmol*. 2019; 22:E9–E60.
67. Hughes A. Topographical relationships between the anatomy and physiology of the rabbit visual system. *J Documenta Ophthalmol*. 1971;30:33–159.
68. Kondo M, Sakai T, Komeima K, et al. Generation of a transgenic rabbit model of retinal degeneration. *Invest Ophthalmol Vis Sci* 2009;50:1371–1377.
69. Huber G, Heynen S, Imsand C, et al. Novel rodent models for macular research. *PLoS One*. 2010;5:e13403.
70. Volland S, Esteve-Rudd J, Hoo J, Yee C, Williams DS. A comparison of some organizational characteristics of the mouse central retina and the human macula. *PLoS One*. 2015; 10:e0125631.
71. Litts KM, Zhang Y, Freund KB, Curcio CA. Optical coherence tomography and histology of age-related macular degeneration support mitochondria as reflectivity sources. *Retina*. 2018;38:445–461.
72. Krebs W, Krebs I. Fine structure of retina. In: *Primate Retina and Choroid: Atlas of Fine Structure in Man and Monkey*. New York: Springer; 1991:160.
73. Carter-Dawson LD, Lavail MM. Rods and cones in the mouse retina. I. Structural analysis using light and electron microscopy. *J Comp Neurol*. 1979;188:245–262.
74. Beauchemin ML. The fine structure of the pig's retina. *Graefes Arch Clin Exp Ophthalmol*. 1974;190:27–45.
75. Adachi K, Takahashi S, Yamauchi K, Mounai N, Tanabu R, Nakazawa M. Optical coherence tomography of retinal degeneration in royal college of surgeons rats and its correlation with morphology and electroretinography. *PLoS One*. 2016;11:e0162835.
76. Zhang QX, Lu RW, Messinger JD, Curcio CA, Guarcello V, Yao XC. In vivo optical coherence tomography of light-driven melanosome translocation in retinal pigment epithelium. *Sci Rep*. 2013;3:2644.
77. Wilk MA, Huckenpahler AL, Collery RF, Link BA, Carroll J. The effect of retinal melanin on optical coherence tomography images. *Trans Vis Sci Tech*. 2017;6(2):8.
78. Kiernan DF, Mieler WF, Hariprasad SM. Spectral-domain optical coherence tomography: a comparison of modern high-resolution retinal imaging systems. *Am J Ophthalmol*. 2010;149:18–31.
79. Tian C, Zhang W, Mordovanakis A, Wang X, Paulus YM. Noninvasive chorioretinal imaging in living rabbits using integrated photoacoustic microscopy and optical coherence tomography. *Optics Express*. 2017;25:15947–15955.
80. Matsuo Y, Sakamoto T, Yamashita T, Tomita M, Shirasawa M, Terasaki H. Comparisons of choroidal thickness of normal eyes obtained by two different spectral-domain OCT instruments and one swept-source OCT instrument. *Invest Ophthalmol Vis Sci*. 2013;54:7630–7636.
81. Ang M, Tan ACS, Cheung CMG, et al. Optical coherence tomography angiography: a review of current and future clinical applications. *Graefes Arch Clin Exp Ophthalmol*. 2018;256:237–245.
82. Gao SS, Jia Y, Zhang M, et al. Optical coherence tomography angiography. *Invest Ophthalmol Vis Sci*. 2016;57:27–36.
83. Kim T-H, Son T, Lu Y, Alam M, Yao X. Comparative optical coherence tomography angiography of wild-type and rd10 mouse retinas. *Trans Vis Sci Tech*. 2018;7(6):42.
84. Liu W, Li H, Shah RS, et al. Simultaneous optical coherence tomography angiography and fluorescein angiography in rodents with normal retina and laser-induced choroidal neovascularization. *Optics Lett*. 2015;40:5782–5785.

Investigative Ophthalmology & Visual Science

85. Park JR, Choi W, Hong HK, et al. Imaging laser-induced choroidal neovascularization in the rodent retina using optical coherence tomography angiography. *Invest Ophthalmol Vis Sci*. 2016;57:OCT331–OCT340.

86. Ollivier FJ, Samuelson DA, Brooks DE, Lewis PA, Kallberg ME, Komaromy AM. Comparative morphology of the tapetum lucidum (among selected species). *Vet Ophthalmol*. 2004;7: 11–22.

Investigative Ophthalmology & Visual Science

Supplementary files

Table S1: Anesthetic procedures

All protocols were designed and approved by veterinary anesthesia and laboratory animal medicine specialists. Thermoregulation was optimized during anesthesia and recovery. None of the animals demonstrated signs of optical axis opacities (cornea, anterior chamber, lens, vitreous). IM (intramuscular), IV (intravenous), CRI (continuous rate infusion), SC (subcutaneous), IP (intraperitoneal).

	Minipigs	Rabbits	Rats	Mice
Sedation:	None	Medetomidine 0.1-0.2 mg/kg IM	None	None
Anesthesia:	Mixture: 25 mg Tiletamine, 25 mg Zolazepam, 12.5 mg Xylazine, 12.5 mg Ketamine, 2.5 mg Butorphanol (per 1 ml) IM in dosage 1 ml per 15 kg	alfaxan bolus 2-4 mg/kg IV followed by alfaxan CRI 2-6 mg/kg/h titrated to effect	Mixture: Fentanyl 0.005 mg/kg, Medetomidine 0.15 mg/kg, Midazolam 2 mg/kg SC	Mixture: Fentanyl 0.05 mg/kg, Medetomidine 0.5 mg/kg, Midazolam 5 mg/kg IP or SC
Reversal:	Atipamezole 0.24 mg/kg IV	Atipamezole 0.25 mg/kg IV	Mixture: Naloxone 0.12 mg/kg, Atipamezole 0.75 mg/kg, Flumazenil 0.2 mg/kg SC or IP	Mixture: Naloxone 1.2 mg/kg, Atipamezole 2.5 mg/kg, Flumazenil 0.5 mg/kg SC or IP
Thermoregulation:	Warming blanket (3M Bair Hugger)	Water circulation heating pad	Water circulation heating pad	Water circulation heating pad
Duration:	Up to 90 min, B-scans presented in the current study acquired within first 20 min	Up to 60 min, B-scans presented in the current study acquired within first 20 min	Up to 60 min, B-scans presented in the current study acquired within first 20 min	Up to 30 min, B-scans presented in the current study acquired within first 10 min

Supplementary files

Table S2: B-scan absolute values for visibility of choriocapillaris and optimal presentation of ORB in all anatomical locations and species.

Compared to the other species examined, the SNR quality of the images from pigmented and albino mice was significantly higher (*) and lower (**), respectively. Age and gender of animals included were dependent on the primary aims of the trials into which the animals were enrolled.

	Minipigs	Rabbits	Rats		Mice	
	Pigmented	Pigmented	Pigmented	Albino	Pigmented	Albino
Total number of evaluated B-scans	128	65	65	128	128	60
Signal-to-noise ratio (SNR)	**28.7**	**29.6**	**29.3**	**29.4**	**32.8***	**26.1****
Total number of animals	20	12	9	24	21	10
Age range	5-8 months	4-6 months	8-16 weeks	7-16 weeks	6-12 weeks	8-12 weeks
Gender	12 M, 8 F	4 M, 8 F	9 M	20 M, 4 F	21 M	10 M
Visibility of choriocapillaris and connecting vasculature						
Total	128/128 (100.0 %)	46/65 (70.8 %)	49/65 (75.4 %)	100/128 (77.7 %)	73/128 (56.5 %)	31/60 (50.8 %)
Dorsal	43/43 (100.0 %)	4/23 (17.4 %)	18/21 (85.7 %)	25/34 (73.5 %)	28/41 (68.3 %)	3/22 (11.4 %)
Central	44/44 (100.0 %)	23/23 (100.0 %)	20/27 (74.1 %)	58/65 (88.5 %)	25/43 (57.0 %)	15/20 (75.0 %)
Ventral	41/41 (100.0 %)	19/19 (100.0 %)	11/17 (64.7 %)	17/29 (58.6 %)	20/44 (45.5 %)	13/18 (72.2 %)
Optimal presentation of outer retinal bands						
Total	15/128 (11.7 %)	48/65 (73.8 %)	52/65 (80.0 %)	37/128 (28.5 %)	117/128 (91.0 %)	38/60 (62.5 %)
Dorsal	12/43 (27.9 %)	8/23 (32.6 %)	18/21 (85.7 %)	11/34 (32.4 %)	33/41 (79.3 %)	11/22 (50.0 %)
Central	1/44 (2.3 %)	23/23 (100.0 %)	20/27 (74.1 %)	21/65 (32.3%)	42/43 (97.7 %)	17/20 (85.0 %)
Ventral	2/41 (4.9 %)	17/19 (92.1%)	14/17 (82.4 %)	5/29 (15.5 %)	42/44 (95.5 %)	10/18 (52.8 %)

Supplementary files

Figure S1: Non-Ideal outer retinal band presentation on SD-OCT B-scans.

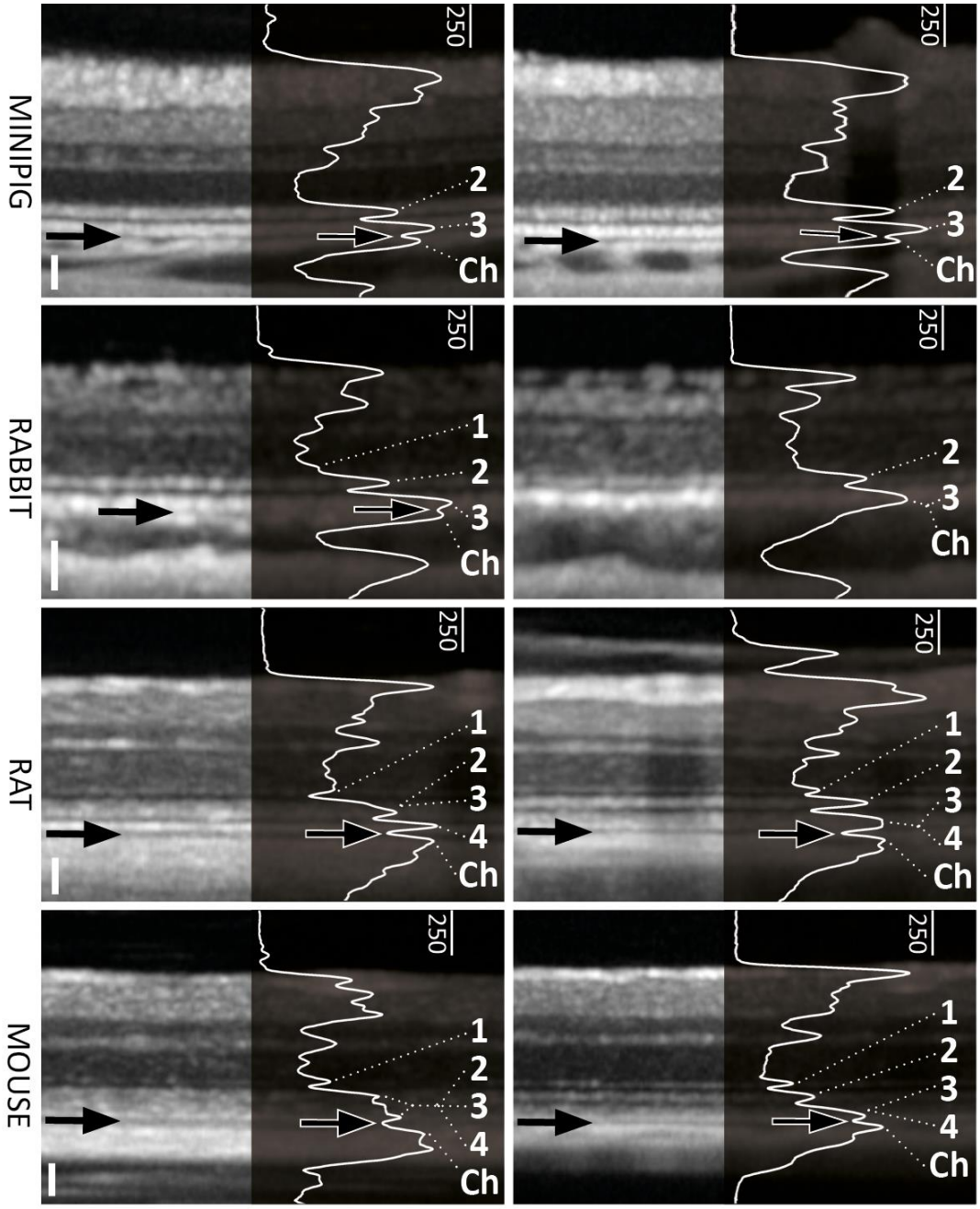

The first ORB representing the ELM was missing on most of the minipig OCTs, with only bands representing the EZ (2) and RPE/BM (3) visible. On rabbit OCTs the first ORB (1) was either indistinct (left) or missing (right). Furthermore, the dip in reflectivity representing the choriocapillaris was often diminished (left) or no distinct border between RPE/BM (3) and choroid (Ch) was visible (right). This was observed most in the scan location dorsal to the ONH. On both rat and mouse OCTs, the border between EZ (2) and IZ (3) (left) or between IZ (3) and RPE/BM (4) (right) was indistinctive or not visible. Black arrows indicate the choriocapillaris in both OCT and reflectivity profile images. OCT location and signal-to-noise ratio: Minipig left: dorsal, 31; right: dorsal, 32. Rabbit left: ventral, 28; right: dorsal, 31. Albino rat left: ventral, 27; pigmented rat right: dorsal, 34. Albino mouse left: dorsal, 27; pigmented mouse right: dorsal, 25. Axial scale bars 50 μm.

Danksagung

Mein aufrechter und herzlichster Dank geht an Prof. Simon Pot für seine langzeitige personale und wissenschaftliche Unterstützung. Unsere Projekte könnten ohne seinen Input und kritische Bewertung nie erfolgreich herauskommen.

Genauso herzlich wollte ich meinem Kollegen aus Humanaugenheilkunde, Dr. Peter Maloca, für seine Visionen und Hilfe danken. Ich bin sehr froh, dass ich bei ihm so viele Sachen im Bereich Augenbildgebungsmethoden lernen durfte.

Dr. Bernd Altmann möchte ich ebenfalls für seine dauernde optimistische Lebenseinstellung und Unterstützung in schwierigen Situationen danken.

Ein weiterer besonderer und grosser Dank geht an meiner lieben Kollegin, Dr. Elke Atzpodien. Sie hat mich von Anfang bis Ende unterstütz und hat in mich geglaubt. Ich werde die zahlreichen Diskussionen und unendliche Unterstützung nie vergessen.

Lieber Simon, Lieber Peter, Lieber Bernd und Liebe Elke, herzlichen Dank!

Zuletzt geht ganz besonderer Dank an meine Frau Alena, ohne ihre Unterstützung wäre ich nicht dort, wo ich bin, und das Leben wäre nicht so spannende Ride!

Curriculum Vitae

Vorname Name	Petr Soukup
Geburtsdatum	2. September 1986
Geburtsort	Frýdlant, Tschechische Republik
Nationalität	Tschechisch
	Schulausbildung
09/1993 – 06/1998	Grundschule Pivovarská, Jablonec nad Nisou, Tschechische Republik
09/1998 – 05/2007	Gymnázium Jablonec nad Nisou, Jablonec nad Nisou Tschechische Republik
09/2004 – 06/2005	West Bend West High School, West Bend, Wisconsin, Vereinigte Staaten von Amerika
	Höchster Schulabschluss
24/05/2007	Abitur, Gymnázium Jablonec nad Nisou, Jablonec nad Nisou Tschechische Republik
	Studium
09/2007 – 09/2013	Veterinärmedizin, Veterinary and Pharmaceutical University Brno, Brünn, Tschechische Republik
	Abschlussprüfung vet. med.
03/09/2013	Veterinärmedizin, Veterinary and Pharmaceutical University Brno, Brünn, Tschechische Republik
02/2017 – 07/2019	**Anfertigung der Dissertation**
	unter Leitung von Prof. Simon Pot, DVM, DACVO, DECVO
	am Departement für Pferde, Abteilung für Ophthalmologie der Vetsuisse-Fakultät Universität Zürich Direktor: Prof. Dr. Colin Schwarzwald, PhD, DACVIM, DECEIM
	Anstellungen nach Abschluss des Studiums
10/2013 – 01/2014	Tierarzt, Dr. Vepřek Kleintierklinik, Mimon, Tschechische Republik
01/2014 – 01/2015	Tierarzt Internship, Pferdeklinik Altforweiler, Altforweiler, Deutschland
02/2015 – 12/2018	Wissenschaftlicher Assistent, Roche Innovation Center Basel, Basel, Schweiz
09/2018 – aktuell	Wissenschaftlicher Assistent, Department für Pferde, Abteilung für Ophthalmologie der Vetsuisse-Fakultät Universität Zürich